PROCEEDINGS OF SPIE

SPIEDigitalLibrary.org/conference-proceedings-of-spie

The lunar laser communication demonstration time-of-flight measurement system: overview, on-orbit performance, and ranging analysis

M. L. Stevens, R. R. Parenti, M. M. Willis, J. A. Greco, F. I. Khatri, et al.

M. L. Stevens, R. R. Parenti, M. M. Willis, J. A. Greco, F. I. Khatri, B. S. Robinson, D. M. Boroson, "The lunar laser communication demonstration time-of-flight measurement system: overview, on-orbit performance, and ranging analysis," Proc. SPIE 9739, Free-Space Laser Communication and Atmospheric Propagation XXVIII, 973908 (15 March 2016); doi: 10.1117/12.2218624

SPIE.

Event: SPIE LASE, 2016, San Francisco, California, United States

The Lunar Laser Communication Demonstration time-of-flight measurement system: overview, on-orbit performance and ranging analysis

M. L. Stevens*, R. R. Parenti, M. M. Willis, J. A. Greco, F. I. Khatri,
B. S. Robinson, D. M. Boroson
Massachusetts Institute of Technology, Lincoln Laboratory
244 Wood Street, Lexington, MA, USA 02124

ABSTRACT

The Lunar Laser Communication Demonstration (LLCD) flown on the Lunar Atmosphere and Dust Environment Explorer (LADEE) satellite achieved record uplink and downlink communication data rates between a satellite orbiting the Moon and an Earth-based ground terminal. In addition, the high-speed signals of the communication system were used to accurately measure the round-trip time-of-flight (TOF) of signals sent to the Moon and back to the Earth. The measured TOF data, sampled at a 20-kS/s rate, and converted to distance, was processed to show a Gaussian white noise floor typically less than 1 cm RMS. This resulted in a precision for relative distance measurements more than two orders-of-magnitude finer than the RF-based navigation and ranging systems used during the LADEE mission. This paper presents an overview of the LLCD TOF system, a summary of the on-orbit measurements, and an analysis of the accuracy of the measured data for the mission.

Keywords: time-of-flight, deep-space navigation, free-space laser communication

1. INTRODUCTION

Deep-space navigation currently is based on microwave radio measurements utilizing tracking stations located throughout the world [1]. One of the key measurements is the round-trip time-of-flight (TOF) of signals sent from the ground station up to the spacecraft and back. These navigation systems are generally designed to use specialized waveforms which require the exclusive use of the satellite RF communication system, supplanting the normal command and telemetry data streams for observation times that often run continuously for hours.

In addition to navigation, time-of-flight measurements are important for planetary science. Gravitational anomalies of planets and moons can be measured by the small perturbations they cause in the position of orbiting spacecraft. The gravitational anomalies can yield important information about the interior of planets and moons [2].

There is a desire to reduce the workload on limited ground terminal resources for the navigation measurements [3]. NASA is currently working on new concepts, including one which can take advantage of the growing number of interconnected satellites in space. This concept allows for autonomous measurements of the spacecraft state vectors utilizing navigation packets sent between satellites linked in a communication network architecture [4].

This paper proposes an alternate novel concept for time-of-flight measurements that was demonstrated on the Lunar Laser Communication Demonstration (LLCD) [5] carried out over 15 days in October and November of 2013. The LLCD time-of-flight used no special waveforms but only the high-speed signals in the duplex communication system. Thus, the time-of-flight data was captured whenever duplex laser communications were in operation.

The Lunar Laser Communication Demonstration Space Terminal was carried on the Lunar Atmosphere and Dust Environment Explorer (LADEE) [6] satellite launched in September 2013. The mission's primary goal was to study the fragile lunar atmosphere and look for the presence of electro-statically transported dust grains. The LADEE satellite was intended to be 100 days in orbit around the Moon. The spacecraft also had sufficient capacity to carry the small experimental laser communication terminal of LLCD.

*Corresponding author: stevens@ll.mit.edu
This work is sponsored by National Aeronautics and Space Administration under Air Force Contract #FA8721-05-C-0002. Opinions, interpretations, recommendations and conclusions are those of the authors and are not necessarily endorsed by the United States Government.

Free-Space Laser Communication and Atmospheric Propagation XXVIII, edited by
Hamid Hemmati, Don M. Boroson, Proc. of SPIE Vol. 9739, 973908 · © 2016 SPIE
CCC code: 0277-786X/16/$18 · doi: 10.1117/12.2218624

During the commissioning phase (the first month in orbit) of the LADEE mission, the spacecraft was placed in a circular orbit about 250 km above the surface of the Moon, and LLCD was allocated about half of the days in the month to exercise the lasercom links. During this period, LLCD demonstrated the longest ever two-way high-rate laser communications, and the first between an Earth-based ground terminal and a satellite orbiting the Moon. A record 622 Mbps communication rate was achieved on the downlink from the Moon to the Earth with a 0.5-W transmitter and 10-cm aperture at the Moon. The ground terminal receiver, located at White Sands, NM used four 40-cm receive telescopes fiber-coupled into four arrays of four super-conducting nanowire single-photon detectors [7]. The ground terminal uplink transmitter used four 15-cm telescopes each fed by a 10-W optical amplifier carrying signals at selectable rates of 10 or 20 Mbps [8]. These uplink data rates were 5000 times higher than the RF-based radios used on all previous missions to the Moon. The increase in data rates made possible by the two-way laser communications enabled real-time high-precision TOF.

During the demonstration, data was streamed to the Moon and back. Data types included multiple simultaneous high-definition video streams, file transfers, commands to the optical terminal at the Moon, and downloads of the entire spacecraft buffer in minutes that would have taken days with the RF telemetry link on the spacecraft.

In addition to the communication demonstration, LLCD also measured the time-of-flight of signals sent to the Moon and back utilizing only the high-speed data clocks implicit in the communication system. No special waveforms were used, so the TOF data was recorded continuously whenever duplex laser communications were in operation. For TOF simplicity, the same framing structure was designed into both the downlink and uplink signals. TOF operation required only that the uplink and downlink clocks be phase-locked to each other, and the framing on the downlink signal be synchronized with the arrival of the frame markers on the received uplink signal at the satellite.

2. LLCD TOF ARCHITECTURE

A block diagram of the laser communication system clocks on board the satellite is shown in Figure 1 [9, 10]. Uplink and downlink data clocks were integer multiples and phase synchronous. A single master clock (VCO) at 5 GHz was phase locked to the received data on the uplink. This same clock was also used to format the data and the modulated waveforms on the downlink. Multiple data rates were selectable on both the uplink and downlink. A fixed duration framing structure was used to transmit the data composed of 1, 2, 4, 8, or 16 time-division-multiplexed sub-channels depending on the selected data rate for the downlink and 8 or 16 sub-channels for the uplink. Each sub-channel was composed of a frame alignment sequence and coded data. The frame duration for the downlink was fixed at 60736 cycles of 311.04 MHz, approximately 195 µs. The uplink used the same frame structure with a fixed duration 32-times the length of the downlink frame, approximately 6.25 ms. The uplink and downlink framing at the satellite terminal were synchronized by a command sent from the ground terminal. These synchronized clocks and framing provided the timing signals that were the basis of the LLCD TOF measurements.

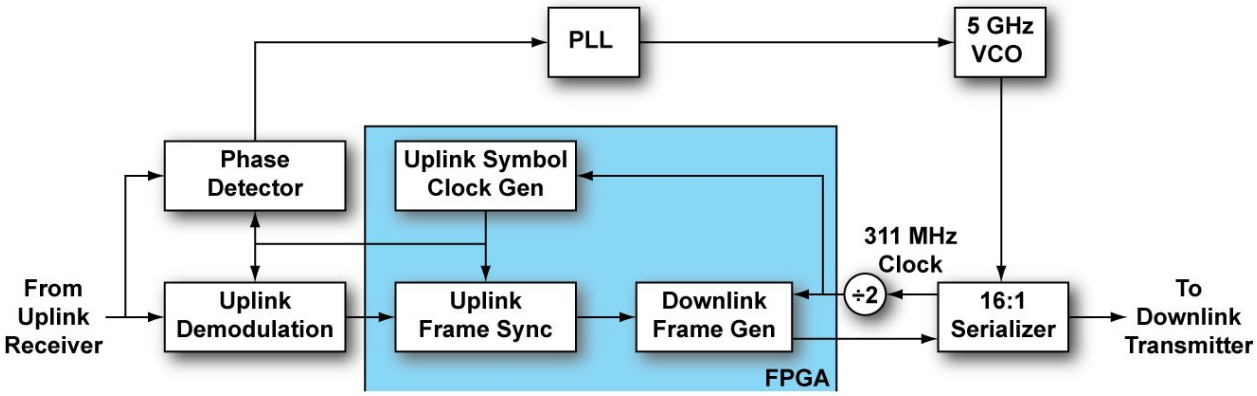

Figure 1. Block diagram of the satellite communication system with TOF measurement capability.

The uplink modulation format was 4-PPM with a fixed slot rate of 311.04 MHz. Each uplink symbol consisted of four slots for the data and an additional 12- or 28-slot dead time where no signal was sent, depending on the selected information rates of either 19.44 Mbps or 9.72 Mbps. (This allowed for a simple, single optical receiver filter.)

The downlink modulation format was 16-PPM with a variable slot rate. At the highest downlink data rate of 622 Mbps, a 4.976 GHz (16 x 311.04 MHz) slot rate was used, the symbol clock being nominally equal to the slot clock on the uplink, but Doppler shifted by the motion of the spacecraft with respect to the ground terminal. Information rates on the downlink were selectable from 622, 311, 156, 78, and 39 Mbps.

A block diagram of the ground terminal communication system clocks is shown in Figure 2 [11]. A low-noise master clock oscillator at 311.04 MHz was used to generate the modulation and framing for the uplink. On the downlink receiver side, a 5-GHz clock was phase locked to the received signal. This recovered downlink clock was divided by 16 to produce the symbol clock at nominally 311.04 MHz, but shifted from the uplink master clock by the two-way Doppler shift resulting from the relative motion of the spacecraft.

Two TOF sensors were built into the downlink receiver yielding so-called "Fine" and "Coarse" data. The Fine data sensor was a phase-frequency detector (PFD) which measured the instantaneous phase difference between the two 311.04 MHz clocks. The PFD had a range of approximately ±300 degrees modulo 360 degrees (one cycle). The analog output of the phase detector was digitized with a 16-bit analog-to-digital converter (ADC) at 20 kS/s, yielding an ADC-limited resolution of approximately 0.023 degrees-per-bit, corresponding to 63µm of round-trip distance.

The Coarse data sensor consisted of a measurement of the time delay between the uplink frame header departures and the downlink frame header arrivals. Downlink frame headers were synchronized at the space terminal to the arrival of the uplink frame headers. This plus the phase-locked uplink and downlink clocks at the satellite resulted in a continuous transfer of timing information over the two-way link at both Fine and Coarse scales. The Coarse delay was measured by clock cycles of the uplink 311.04 MHz master clock. This measurement, providing coarse two-way TOF data, was sampled at 160 S/s with a resolution of 1 cycle at 311.04 MHz, equivalent to approximately 0.96 m. The maximum time delay measurable by the system was the duration of a downlink frame, 60736 cycles of 311.04 MHz, or about 195 µs, resulting in a range ambiguity of approximately 58.5 km. This ambiguity was resolved during LLCD using ephemerides provided by the LADEE navigation team for LLCD terminal pointing and acquisition. (Future systems could incorporate numbered uplink frame headers or unique uplink data payload markers that could be looped back from the uplink to the downlink at the satellite terminal, if eliminating the ambiguity is required.)

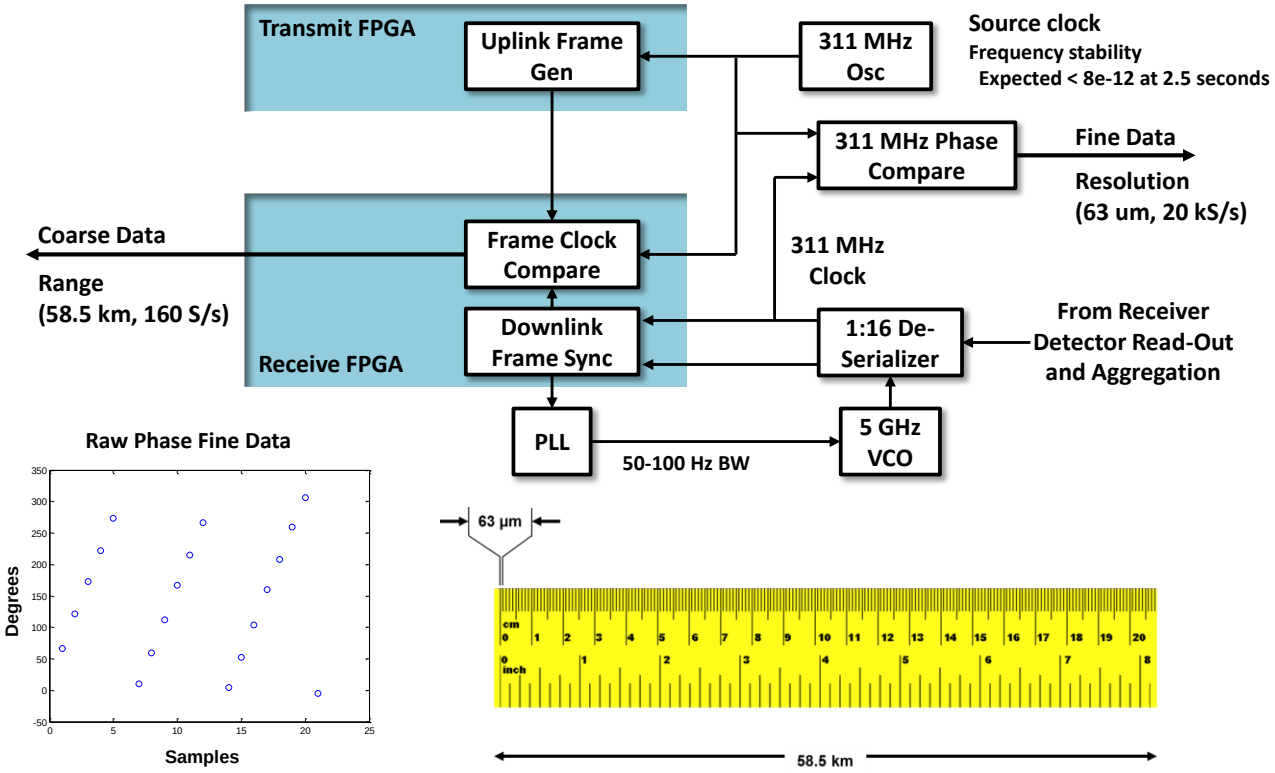

Figure 2. Block diagram of the ground-based clock system with TOF measurement capability.

The Coarse and Fine data provided LLCD with a ruler to measure round-trip TOF with an equivalent length of 58.5 km and a smallest 'tick' mark of 63µm.

We note that the Fine data alone could be used to generate precision cumulative phase measurements which give rise to relative two-way TOF or distance measurements. Absolute measurements are obtained by adding the offset bias obtained from the Coarse data (after resolving the ambiguity using ephemeris predictions and after carefully accounting for latencies in the ground and satellite terminals.)

3. TOF DATA PROCESSING

The Fine data sensor output was first processed to deduce the relative TOF (equivalent to differential distance) by unwrapping the modulo-360-degree data, a sample of which is shown in Figure 3. Each sawtooth corresponds to one cycle of 311.04 MHz. At the Doppler null (at closest approach of the satellite to the ground terminal) the phase change can be seen to slow and reverse direction. The range of the phase frequency detector was about 600 degrees. Thus, when the phase reached +300 degrees it rolled over to -60 degrees, and when the phase reached -300 degrees it rolled over to +60 degrees. This resulted in a simple linear relationship between the detector output and phase. A cumulative-phase time series was thus generated from the raw ADC samples after conversion to degrees. The cumulative phase was arbitrarily defined to start at 0 and end with the total cumulative phase over the measurement interval, which we defined as the period of duplex communications with continuous phase locking of both the uplink and downlink receiver clocks (and which was typically a quarter up to the full 20-25 minute pass defined by the LADEE orbit and depending on the number of communication system parameters chosen for test during the pass.) Artifacts caused by samples that fell in the rollover regions were smoothed by applying a simple straight line interpolation at every rollover in the unwrapped cumulative-phase time series. It was also known that the PFD exhibited a slight non-linearity in its measurements near the extremes of its range. Residual errors from the smoothing and non-linearity thus led to some feed-through of the beat-frequency difference between the two clocks, but which we removed by filtering after processing. (An example of the residuals with beat-frequency noise before and after filtering is shown in Figure 7 in section 4.1).

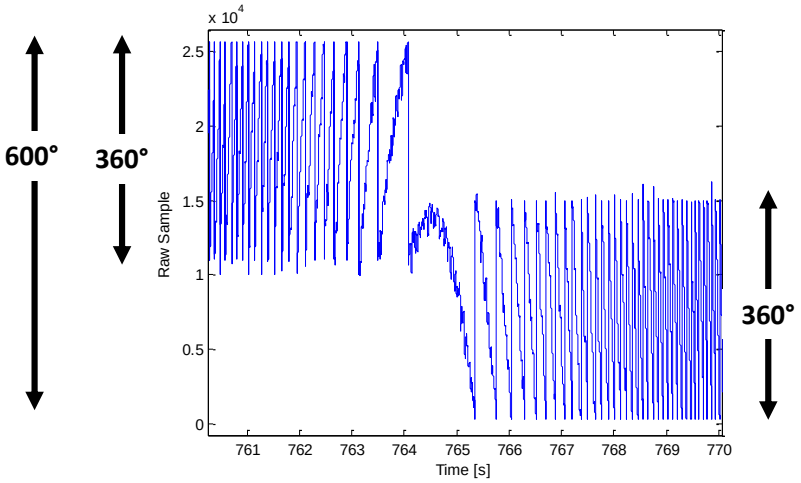

Figure 3. The PFD measures the instantaneous phase difference of the two 311.04 MHz clocks. Each sawtooth is one cycle of 311.04 MHz. The phase change slows and then reverses direction at the Doppler null where the satellite makes its closest approach.

Figure 4 (a) shows this cumulative phase converted to one-way relative distance (red) and overlaid on the relative distance predictions from the operational satellite ephemeris (blue). On this scale the total change in distance during this 10-minute measurement interval is seen to be about 90 km. An excellent fit with the ephemeris (on such a distance scale) can be seen.

We are next interested in the residual noise and variations in our measurements. Spacecraft navigation teams typically perform this step by creating multi-parameter orbital, gravity, and trajectory models and then perform best fits of these to

the TOF data. As this complex calculation was not part of the LLCD mission, we decided to approximate such results by subtracting a polynomial fit (i.e. an approximation to an orbit) from the measured data. Sample residuals are shown in Figure 4 (b)[†]. The noise deduced by such measurements (before any filtering) were found in this particular data set to be equivalent to 127 ps or 3.8 cm RMS in round-trip distance.

We then performed this approximate analysis on the data from the entire mission (approximately 100 total passes). We calculated the standard deviation in each 1-second block (to minimize the effects of polynomial fitting errors) and averaged over all such intervals to produce the values shown in Figure 5. Averaging over all mission data resulted in 44.3 ps or 1.3 cm (shown by the solid line) for the two-way TOF.

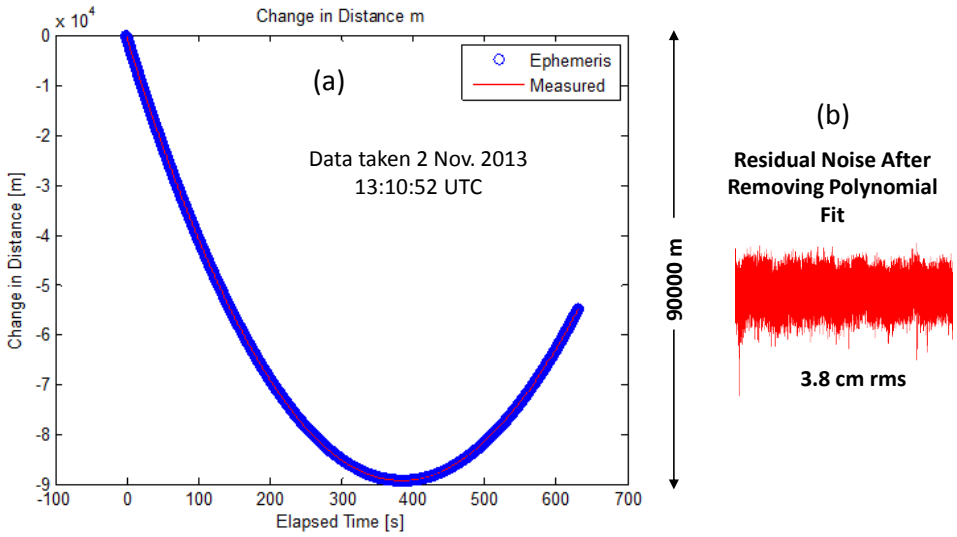

Figure 4. Overlay of measured cumulative phase converted to one-way distance and ephemeris prediction.

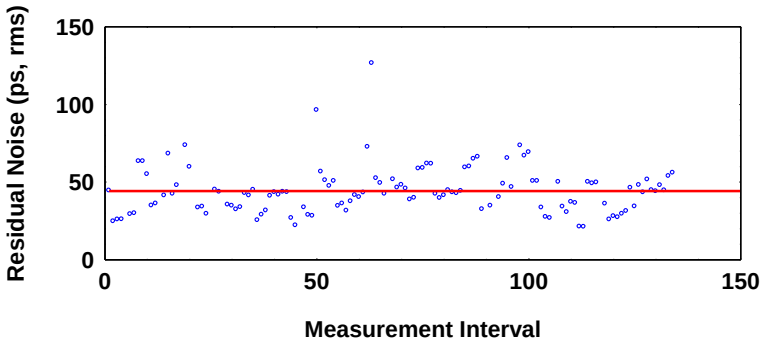

Figure 5. Standard deviation of noise in two-way TOF measurements for the mission. Average for the mission (Red) was 44.3 ps, equivalent to a two-way distance error of 1.3 cm.

Absolute distance measurements were extracted by adding the absolute bias offset from the Coarse data to the Fine data time series. We calculated the absolute TOF offset by first down sampling and interpolating the Fine data to the same sampling times as the Coarse data. We then computed the mean difference, over a measurement interval, between the Coarse data (including corrections for the terminal latencies and resolution of the Coarse data ambiguity) and the unwrapped interpolated Fine data. Taking the mean of the difference of many Coarse-Fine data pairs allowed us to

[†] Additional processing was performed to remove artifacts caused by a GPS receiver that was used as the reference clock for the ground terminal. Details are provided in Appendix A.

achieve high precision absolute offsets. The quantization noise in the Coarse data has the variance of a uniform distribution over one cycle of 311.04 MHz (σ^2 = 0.0768 m^2). This variance is reduced, though, by the reciprocal of the number of Coarse samples in the measurement (at 160 samples per second.) The expected error in the absolute offset for a typical measurement interval of 100–1000 seconds was thus shown to be 2.2 – 0.7 mm RMS‡. We then added this absolute offset to the original Fine data time series to produce an absolute two-way TOF. (We note that only a single absolute offset value is required for any period where the Fine data is continuous.)

4. COMPARISONS WITH LADEE EPHEMERIS

Finding a "truth" against which to compare an absolute range measurement is difficult. We used the LADEE ephemeris data in this comparison. Because the ephemeris samples provided by LADEE came once every five seconds (or greater), much interpolation was required to compare that data with the LLCD TOF data. We used polynomial, spline, and other fitting methods for this exercise, knowing full well that a real orbit/trajectory modeling approach would be required to give the best results.

4.1 Characterization of the Time-Of-Flight range noise

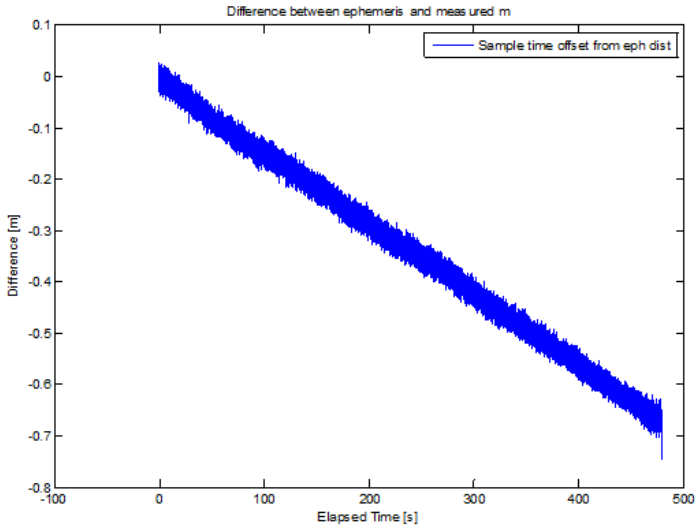

Figure 6. Difference between the one-way change in ephemeris distance and the one-way change in link distance derived from the time-of-flight measurements.

Our analysis of the range data generated from the Fine data, shown earlier, has shown a Gaussian noise component that is consistent with the 1.3 cm accuracy limit of the round-trip TOF. There are, however, other error sources as well, which we will discuss by examining a representative data set, (recorded on 20 Oct. 2013 at 02:13:29 UTC). The function plotted in Figure 6 represents the difference between the receiver differential range estimates for this data sample and the high-rate interpolation to NASA's ephemeris calculations. To properly assess the characteristics of the noise in the TOF time series plotted in Figure 6, several steps were taken to isolate random measurement errors from non-random data artifacts. As described earlier and illustrated in Figure 7, the raw data include an additive component due to the beat-frequency output of the PFD. Since these high-frequency fluctuations lie outside the bandwidth of the measurement noise, their impact can be minimized through the use of a relatively low-pass filter. We deduced that a

‡ Our GPS receiver, used as a clock reference in the ground terminal, did not meet its assumed specification and produced artifacts described in Appendix A, resulting in additional uncertainty in the absolute offset. The GPS receiver frequency stepping produced an equivalent two-way distance variance of σ^2 = 0.21 m^2. Averaging reduced the variance by the reciprocal of the number of independent 10-second frequency steps in a measurement interval. Including the GPS receiver artifacts, the expected error for our absolute offset was 14.4 – 4.6 cm RMS for a typical measurement interval of 100 – 1000 seconds. But we believe the 2.2 – 0.7 mm value stated here will be valid for future systems.

200-Hz filter was a good trade between removing these artifacts and not destroying useful TOF data. The output of a 200-Hz Butterworth filter is illustrated by the red overlay in Figure 7.

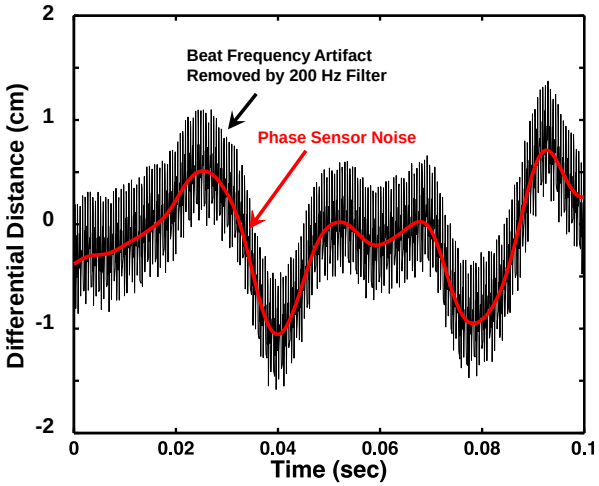

Figure 7. One-way time-of-flight measurement segment showing the high-frequency noise component (black trace) and the result of low-pass (200 Hz) filtering (red curve).

In order to further isolate the noise terms, we removed slow, linear components of the signal to produce a time series having a zero mean and slope. Figure 8 shows the resulting histogram (black curve) and its best-fit Gaussian function, which was found to have a standard deviation of 0.93 cm (red curve) for the one-way TOF for this example. This is a precision for relative distance measurements more than two orders-of-magnitude finer than the RF-based navigation and ranging systems used during the LADEE mission. In future systems, low-pass filtering could be employed to further reduce these estimate uncertainties, suggesting that millimeter-class range accuracies should be achievable in similar TOF systems with time-average sampling rates below 1 Hz.

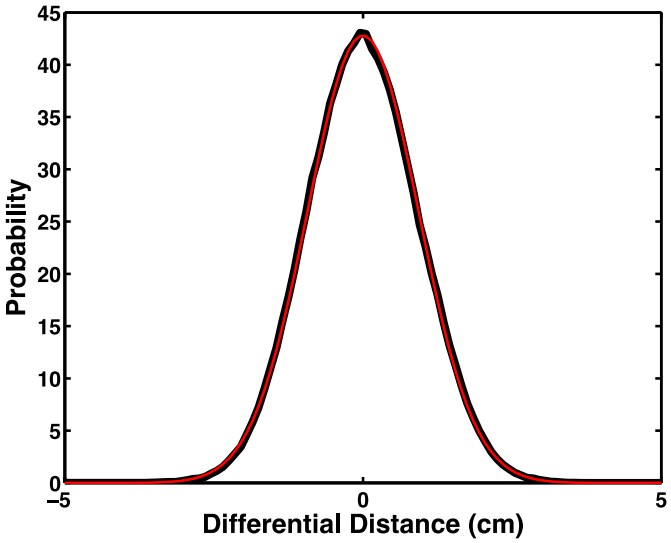

Figure 8. One-way residual noise probability density function. The red overlay indicates a best fit Gaussian function for a standard deviation of 0.93 cm.

From this residual noise data, we also calculated the noise power spectrum, which is shown in Figure 9, and which is approximately white between DC and 20 Hz.

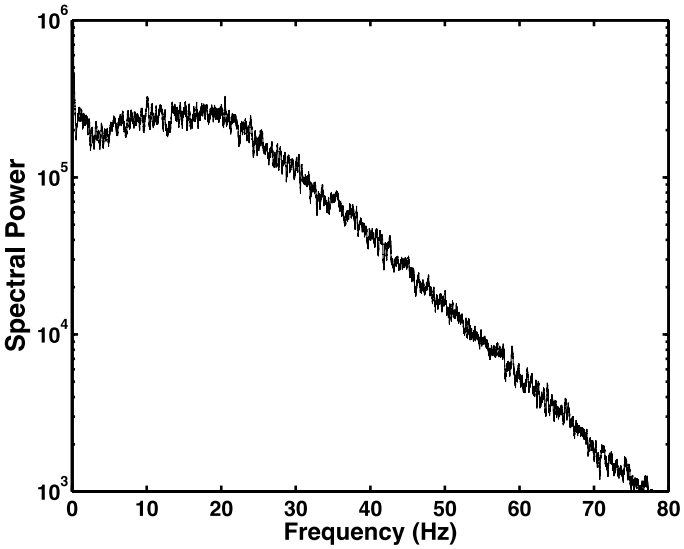

Figure 9. One-way residual noise power spectrum showing a white noise behavior out to 20 Hz.

4.2 Further discussion of the comparison with LADEE ephemeris

Using our method of range analysis, we compared our data with ephemeris-based calculations. When we did this, we found (see Figure 6) differences of up to a few meters in some passes lasting tens of minutes.

We can think of three possible reasons for such a non-zero slope of the distance signal. First, the slope component, which in Figure 6 corresponds to 1 mm/sec drift from the predicted ephemeris, could be attributed to errors in the ephemeris data table or the interpolation of that data. Second, there could be an accumulated bias error in our time-of-flight measurement. Third, there could be a temporal offset between the ephemeris table and the phase sampling system.

If we remove this slow linear component from each pass, we are left with a new type of variation in some of the data files, which is possible evidence of real (small) satellite motions relative to the predicted orbital model. We show one example of this in Figure 10, whose data was recorded on 21 Oct. 2013 at 10:44:59 UTC. We have removed the linear term from this data, and have applied a further 0.2-Hz Butterworth filter. We see in Figure 10 that several centimeter-scale displacements remain. These features have time scales of the order of 100 seconds, which corresponds to orbital distances of about 100 km.

We have looked at four possible causes for these variations. First, drift in the 311.04 MHz master oscillator could account for the variations but we have found that only a few measurement intervals exhibit this feature. Oscillator drift would be expected to be a feature of all the measurement intervals if it was a significant factor[§]. A second possibility could be platform movement in terms of roll, pitch, and yaw (i.e., motion of the LLCD terminal with respect to the center of mass of LADEE.) But the variations we see here are orders of magnitude greater than would be expected from known platform movements. A third possibility could be a temperature variation somewhere in our system. But our pre-launch data showed a very linear correlation between temperature and phase. Looking at the archived temperature telemetry, we found that the measured temperature change during this period was monotonic, and so likely did not cause the variations found. Finally, we found that signal power variations can cause phase changes under certain conditions. But, again, archived telemetry of received signal power at the space terminal showed no correlation with the measured phase variations.

[§] The frequency stepping of the GPS reference receiver described in Appendix A was a feature of all of the measurement intervals, but this disturbance was periodic in nature and was removed from the Fine data.

Thus, we have reason to believe that the measured several centimeter offset from the ephemeris calculation is real, perhaps having something to do with Lunar gravity anomalies, orbital relativistic effects, Earth tidal forces, or actual spacecraft motions.

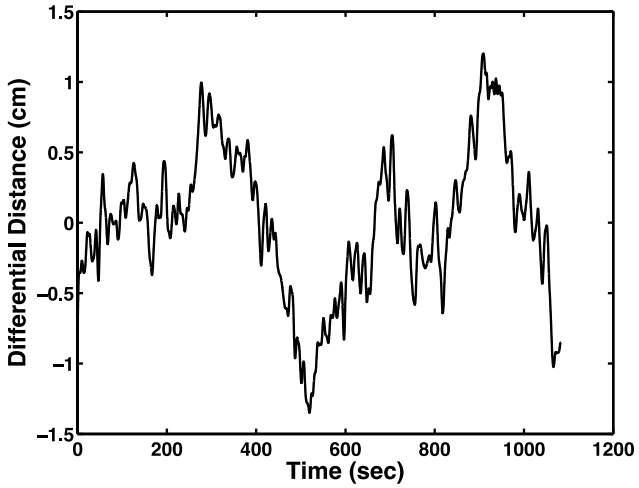

Figure 10. Low-frequency variations observed in a one-way differential measurement following the removal of the linear slope components and the application of a 0.2-Hz temporal filter.

5. SUMMARY

LLCD demonstrated record uplink and downlink data rates between a satellite orbiting the Moon and an Earth-based ground terminal. These high data rates, implemented on LLCD with optical links, enabled precision two-way TOF measurements using only the communication signals. The LLCD TOF system made real-time phase comparisons of the uplink and recovered downlink signals, and yielded a precision in relative one-way distance measurements typically better than 1 cm RMS with real-time samples at 20 kS/s and 200 Hz filtering. This resulted in a precision for relative distance measurements more than two orders-of-magnitude finer than the RF-based navigation and ranging systems used during the LADEE mission. We have also found that additional filtering could be applied to yield millimeter precision. LLCD TOF measurements were generated and archived whenever duplex communications were established during the month of LLCD operations, and required no special navigation waveforms or data in the communication stream. We believe that such high-rate communication-signal-based time-of-flight systems could be highly useful in future navigation and science missions.

APPENDIX A: GPS RECEIVER ARTIFACTS

We used a commercial GPS receiver (not specially designed for the LLCD TOF system) to provide the 10-MHz reference clock signal at the ground terminal that generated the master clock at 311.04 MHz as well as the time-of-day clock used to time stamp the TOF data. Internal to the GPS receiver, the local 10-MHz clock oscillator was periodically trimmed by comparison to the Global Positioning Satellite system atomic clocks, and gave performance known to approach the long-term accuracy of the GPS atomic clocks. But the firmware in the particular GPS receiver unit that was used for LLCD operations actually updated its local clock every 10 seconds resulting in random part-per-billion shifts in the reference clock frequency at 10.000 MHz. (Because of this, the unit did not meet its assumed specification during the mission, but this was not discovered until after the mission was over.) The result of each such frequency step was an apparent ramp in phase, which corresponded to distance on the order of a meter for the approximate 2.6-second round-trip time of the 311.04 MHz master clock signal from the Earth to the satellite orbiting the Moon and back.

The standard deviation of the frequency stepping at the 10.000 MHz reference was found to be typically 0.00588 Hz RMS as measured in a typical segment, a portion of which is shown in Figure 11. At the 311.04 MHz master clock this resulted in 0.183 Hz RMS deviations. Over the approximate 2.6-second round-trip TOF this resulted in apparent distance changes of:

$$\sigma = \frac{0.183 \cdot 2.6 \cdot c}{311.04e6} = 0.458 \text{ meters RMS,} \tag{1}$$

where c is the speed of light. Again, we discovered that this error had happened regularly, every 10 seconds. Such frequency-stepping resulted in large step variations in the residual two-way phase, shown in the example in Figure 12. The residual TOF phase was generated by subtracting twice the predicted ephemeris distance, converted to phase, from the measured two-way cumulative phase. (Such a subtraction from the data was used in order to keep the residual signal to be processed to be only a few meters. The same TOF data used in this example was shown in Figure 4 with a total range change of approximately 90 km.)

A simple model of the measured TOF data converted to two-way distance has the following components:

$$R_m = N + R_a + \frac{c}{f_0}\int f_{step}(t) - f_{step}(t - \tau_{TOF})dt\,. \tag{2}$$

Here, R_m is the measured two-way range, N is the noise floor described earlier, R_a is the actual two-way range, and the phase change due to frequency-stepping is given by the integral where the frequency step is defined by:

$$\begin{aligned} f_{step} &= 0 \quad t < t_0 \\ f_{step} &= f_1 \quad t \geq t_0 \end{aligned}, \tag{3}$$

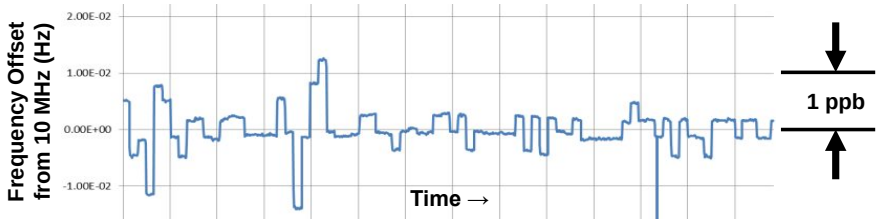

Figure 11. Frequency plot of 10.000 MHz GPS reference oscillator.

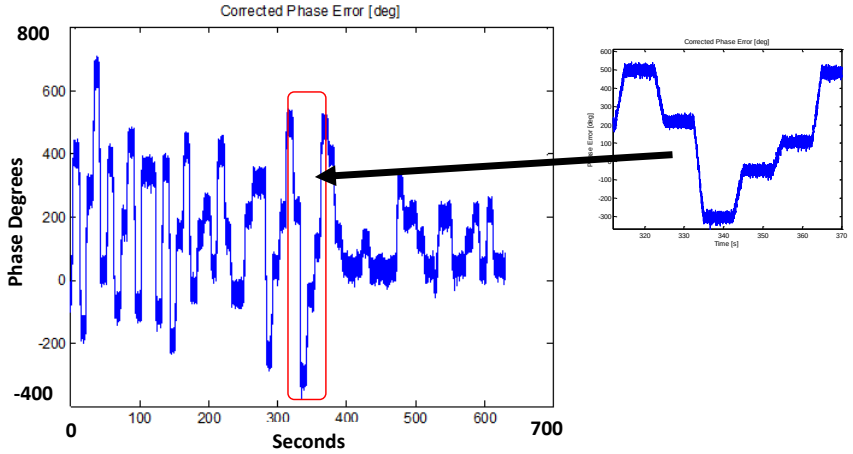

Figure 12. Residual two-way phase error at 311.04 MHz after subtracting twice the predicted ephemeris distance (converted to phase) from the measured TOF data. Frequency stepping of the GPS reference clock is revealed as apparent ramps in phase.

with f_1 defined to be the (random) step inserted by the clock in this particular 10-second interval. The PFD measures the phase difference between the outgoing clock at time t and the returned clock which carries this frequency-step information at time t-τ_{TOF}. The quantity inside the integral has the values:

$$\begin{aligned} f_{step}(t) - f_{step}(t-\tau_{TOF}) &= 0 \quad t < t_0 \\ f_{step}(t) - f_{step}(t-\tau_{TOF}) &= 0 \quad t > t_0 + \tau_{TOF} \\ f_{step}(t) - f_{step}(t-\tau_{TOF}) &= f_1 \quad t_0 \le t \le t_0 + \tau_{TOF} \end{aligned} . \tag{4}$$

Another frequency step occurs ten seconds later at time t_0 +10 with a new value for f_1. We subtracted the predicted ephemeris distance, R_e, from R_m to remove as much as possible the actual range, R_a, from the measurement leaving only noise and the frequency stepping as shown in the residual phase plot in Figure 12.

$$R_m - R_e = N + R_a - R_e + \frac{c}{f_0}\int f_{step}(t) - f_{step}(t-\tau_{TOF})dt \,. \tag{5}$$

Our correction of the frequency stepping was aided by knowledge of the exact 10-second periodicity of the step. We first used a 10000-point (~0.5-second) running average to reduce the noise. The frequency step f_1 was then estimated by differentiating to determine the linear slope component between t_0 and $t_0+\tau_{TOF}$.

$$f_1 = f_{step}(t_0) - f_{step}(t_0 - \tau_{TOF}) \approx \left[\frac{f_0}{c}\frac{d(R_m - R_e)}{dt}\right]^{t=t_0} . \tag{6}$$

We then integrated this estimate of the frequency change over the approximate 2.6 second round-trip TOF to derive the distance correction

$$R_{corr} = R_m - \frac{c}{f_0}\int_{t_0}^{t_0+\tau_{TOF}} f_1 dt \,. \tag{7}$$

Good accuracy was achieved with this correction process where agreement between predicted ephemeris distance and our measurements was observed such that between t_0 and $t_0+\tau_{TOF}$

$$\frac{d(R_a - R_e)}{dt} << \frac{c}{f_0} f_1 \,. \tag{8}$$

We observed this to be the case for most of our measurements where the 10000-point running average was expected to suppress the noise (σ) in the correction 20-dB below the residual noise floor of the measurement. We applied our frequency step correction only over the 2.6-second round-trip time during which the PFD produced the phase ramp.

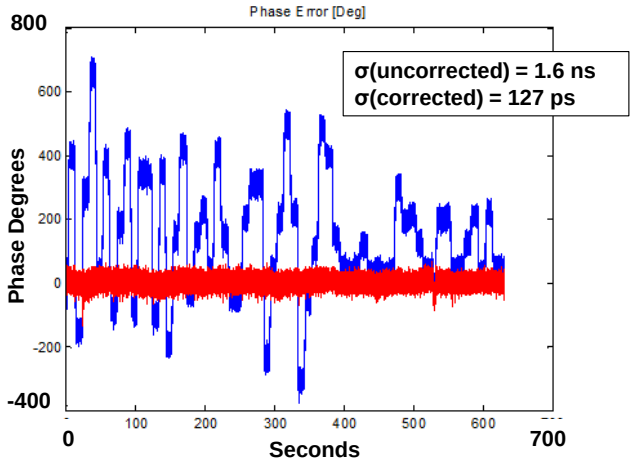

Figure 13. Residual two-way phase error at 311.04 MHz before (black, blue on-line) and after (gray, red on-line) frequency-step correction.

Figure 13 shows the residuals before (black, blue on-line) and after (gray, red on-line) we applied the frequency-step correction to the measured data which was used to generate the residuals shown in Figure 12. We subtracted a best-fit

polynomial from the corrected data to generate the residuals after correction (red). The corrected residuals over this >600 second measurement have a standard deviation of 127 ps, equivalent to 3.8 cm for the two-way TOF for this example[**]. Thus, although this unplanned error in the hardware complicated our TOF calculation, we believe that our correction method was valid, that the LLCD TOF system still demonstrated the great accuracy possible with such a system, and that careful long-term pre-operations calibration can simplify the data processing in future systems.

We gratefully acknowledge the assistance of David O. Caplan, David J. Geisler, and Stephan P. Bedrosian for assistance in this analysis.

REFERENCES

[1] J. B. Berner, S. H. Bryant, and P. W. Kinman, "Range Measurements as Practiced in the Deep Space Network," Proceedings of the IEEE, 95(11), 2202-2214 (2007).

[2] F. G. Lemoine, S. Goossens, T. J. Sabake *et al.*, "High-degree gravity models from GRAIL primary mission data," Journal of Geophysical Research: Planets, 118, 1676-1699 (2013).

[3] J. Hamkins, P. W. Kinman, H. Xie *et al.*, "Telemetry Ranging: Concepts," IPN Progress Report, 42-203, (2015).

[4] E. Anzalone, C. Becker, D. Crump *et al.*, "Multi-spacecraft Autonomous Positioning System: LEO Demo Development," Small Satellite Conference, (2015).

[5] D. M. Boroson, B. S. Robinson, D. V. Murphy *et al.*, "Overview and Results of the Lunar Laser Communication Demonstration," Proc. SPIE, 8971, 1-11 (2014).

[6] R. C. Elphic, and C. Russell, [The Lunar Atmosphere and Dust Environment Explorer Mission (LADEE)] Springer International Publishing, Switzerland (2015).

[7] M. E. Grein, A. J. Kerman, E. A. Dauler *et al.*, "An optical receiver for the Lunar Laser Communication Demonstration based on photon-counting superconducting nanowires," Proc. SPIE, 9492 1-6 (2015).

[8] D. O. Caplan, J. J. Carney, R. Lafon *et al.*, "Design of a 40 Watt 1.55 um Uplink Transmitter for Lunar Laser Communications," Proc. SPIE, 8246, (2012).

[9] M. L. Stevens, and D. M. Boroson, "A simple delay-line 4-PPM demodulator with near-optimum performance," Optics Express, 20(5), 5270-5280 (2012).

[10] S. Constantine, L. E. Elgin, M. L. Stevens *et al.*, "Design of a high-speed space modem for the Lunar Laser Communications Demonstration," Proc. SPIE, Free-Space Laser Communication Technologies XXIII, 7923, (2011).

[11] M. M. Willis, B. S. Robinson, M. L. Stevens *et al.*, "Downlink synchronization for the lunar laser communications demonstration," International Conference on Space Optical Systems and Applications (ICSOS), 83-87 (2011).

[**] The corrected residuals are also shown in Figure 4 (b).